

Spin dynamics in the second subband of a quasi-two-dimensional system studied in a single-barrier heterostructure by time-resolved Kerr rotation

F. ZHANG, H. Z. ZHENG^(a), Y. JI, J. LIU and G. R. LI

State Key Laboratory for Superlattices and Microstructures, Institute of Semiconductors, Chinese Academy of Sciences - P.O. Box 912, Beijing 100083, China

received 27 March 2008; accepted in final form 25 June 2008
published online 6 August 2008

PACS 72.25.Fe – Optical creation of spin polarized carriers
PACS 72.25.Dc – Spin polarized transport in semiconductors
PACS 78.47.-p – Spectroscopy of solid state dynamics

Abstract – Spin dynamics in the first and second subbands have been examined simultaneously by time resolved Kerr rotation in a single-barrier heterostructure of a 500 nm thick GaAs absorption layer. By scanning the wavelengths of the probe and pump beams towards the short wavelength in the zero magnetic field, the spin coherent time T_2^{1*} in the 1st subband E_1 decreases in accordance with the D'yakonov-Perel' (DP) spin decoherence mechanism. Meanwhile, the spin coherence time T_2^{2*} in the 2nd subband E_2 remains very low at wavelengths longer than 810 nm, and then is dramatically enhanced afterwards. At 803 nm, T_2^{2*} (450 ps) becomes ten times longer than T_2^{1*} (50 ps). A new feature has been discovered at the wavelength of 811 nm under the bias of -0.3 V (807 nm under the bias of -0.6 V) that the spin coherence times (T_2^{1*} and T_2^{2*}) and the effective g^* factors ($|g^*(E_1)|$ and $|g^*(E_2)|$) all display a sudden change, presumably due to the "resonant" spin exchange coupling between two spin opposite bands.

Copyright © EPLA, 2008

The behaviors of spin coherence in both bulk semiconductors and their low-dimensional quantum structures have been extensively studied [1] in order to make it feasible in the future that the spin degree of freedom can be employed as an alternative carrier of information in the next generation electronics. Most of experimental investigations have been focused on the dynamics of spin decoherence in ground states [2]. However, few of them concerned the spin coherence in excited states. It was theoretically predicted that due to the strong inter-subband scattering, the spin decoherence rate of electrons in ground and excited subbands were almost identical, despite the large difference in the D'yakonov-Perel' (DP) terms of different subbands [3]. Meanwhile, the spin decoherence rate in the second subband was found to be much slower than in the first subband due to a small spin-orbit splitting at small Fermi wave vectors in the weakly occupied second subband [4]. To clarify the spin dynamics in the second subband, it is desirable to directly observe the temporal spin evolutions in the second subband as it is in the first subband.

In this work, the population in the second subband is created by drifting the spin-polarized electrons, excited in the 500 nm thick GaAs layer by circularly polarized pump pulse, into the vicinity of an AlAs barrier in a single-barrier heterostructure, thus simultaneously occupying the 1st and 2nd subbands in a quasi two dimensional electron system (Q2DES). This enables us to detect the spin dynamics in both subbands by the time resolved Kerr rotation (TRKR).

The sample structure for this investigation was a single-barrier tunneling diode, grown by molecular beam epitaxy (MBE) with a thick intrinsic GaAs as the absorption layer. The layer structures, sample preparation, and measurement configuration for the time resolved Kerr rotation (TRKR) were the same as in ref. [5].

Before disclosing the experimental data, we first briefly give the derivation of the Kerr rotation [6], which is suitable in the case of TRKR measurements. In the reflection configuration, the Kerr angle θ_k and the ellipticity η_k are defined as

$$\theta_K = -\text{Im} \frac{N_+ - N_-}{N_+ N_- - 1}, \quad \eta_k = \text{Re} \frac{N_+ - N_-}{N_+ N_- - 1}. \quad (1)$$

^(a)E-mail: hzzheng@red.semi.ac.cn

Here, $N_{\pm} = n_{\pm} + ik_{\pm}$ are the complex refraction indexes for two circularly polarized lights σ^{\pm} , respectively. The Kerr angle θ_K and the ellipticity η_K can be directly related to the real (χ'_{xy}) and imaginary (χ''_{xy}) parts of the off-diagonal matrix elements for dielectric susceptibility χ_{xy} in the forms

$$\theta_K = -\frac{\chi'_{xy}}{n(n^2+1)} \quad \text{and} \quad \eta_K = -\frac{\chi''_{xy}}{n(n^2-1)} \quad (2)$$

Below, we only consider the specific case where an ordinary (nonmagnetic) semiconductor is first excited by a circularly polarized pumping pulse, which creates imbalanced density functions ρ_p^{\pm} and ρ_m^{\pm} for the spin-polarized states in the final up-band p and the initial low-band m . The semiconductor is then probed by a linearly polarized probe pulse. By following Kubo's formulism [6], we generalize the matrix element for the dielectric susceptibility $\chi_{\mu\nu}(\omega)$ in the following manner:

$$\chi_{xy}(\omega) = \frac{-i}{4V\hbar} \lim_{\eta \rightarrow 0^+} \left\{ \sum_{m,p} (\rho_m - \rho_p)_+ \times \frac{|M_+|_{mp}^2}{\omega_p - \omega_m - \omega - i\eta} - \sum_{m,p} (\rho_m - \rho_p)_- \times \frac{|M_-|_{mp}^2}{\omega_p - \omega_m - \omega - i\eta} \right\}. \quad (3)$$

Here, the density functions are decomposed into spin-majority $(\rho_m - \rho_p)_+$ and spin-minority $(\rho_m - \rho_p)_-$ parts. For the squared matrix elements of the σ^{\pm} -polarized interband transitions $|M_+|_{mp}^2 = |M_-|_{mp}^2$ in the vicinity of the band gap in an ordinary semiconductor. Then, the real part of χ_{xy} is modified as

$$\chi'_{xy}(\omega) = \frac{-\pi}{4V\hbar} \sum_{m,p} (\rho_{p+} - \rho_{p-}) \times |M_{\pm}|_{mp}^2 \delta(\omega_p - \omega_m - \omega). \quad (4)$$

The summation over the states m in the low-band and the states p in the up-band can be replaced by the summation over k -space, as it is conventionally done to account for the contributions from all the interband transitions that are allowed by the energy- and momentum-conservation rule. We find that

$$\theta_K = -\frac{\varepsilon'_{xy}}{n(n^2-1)} = \frac{1}{n(n^2-1)} \frac{|M_{\pm}|_{vc}^2}{16\pi} \left(\frac{2m_r}{\hbar^2} \right)^{\frac{3}{2}} \times \sqrt{\hbar\omega - E_g} \left[\frac{1}{1 + e^{\frac{\hbar\omega - E_g - \mu_F^+}{k_B T}}} - \frac{1}{1 + e^{\frac{\hbar\omega - E_g - \mu_F^-}{k_B T}}} \right]. \quad (5)$$

Here, we employ the quasi-equilibrium assumption that ρ_{c+} and ρ_{c-} can be replaced by respective quasi-Fermi distributions in spin-majority and spin-minority bands with different quasi-Fermi levels μ_F^{\pm} in the conduction band.

Based on the above expression, let us check what happens at $T = 0$ K. a) When $(\hbar\omega - E_g)$ is less than μ_F^{\pm} , χ'_{xy} and θ_K equal zero; b) when $\mu_F^- < \hbar\omega - E_g < \mu_F^+$, θ_K has

a nonzero positive value; c) when $(\hbar\omega - E_g)$ is larger than μ_F^+ , χ'_{xy} and θ_K again equals zero. All of these predictions are in accordance with the experimental observations so far.

In our recent work [5], we demonstrated that, instead of the Rashba and Dresselhaus types, a dynamic spin splitting along the growth direction can be induced in heterostructures when a population imbalance between two electron spin bands is created by a circularly polarized excitation. This is because the single-particle energy of an electron will be renormalized due to its exchange interaction with other electrons in interaction electron gas. The difference between the renormalized energy of the majority and minority spin bands creates an observable dynamic spin splitting. In the presence of spin splitting induced by exchange self-interaction, the effective band gap of the majority spin band (+) becomes smaller than that of the minority spin band (-) by an amount of $E_g^- - E_g^+ = |\Delta E_{ex}(k, 0)|$, where $\Delta E_{ex}(k, 0)$ is the difference in the static exchange self-energies of the minority and majority spin bands. Then, the Kerr rotation takes a slightly modified form

$$\theta_K = -\frac{\varepsilon'_{xy}}{n(n^2-1)} = \frac{1}{n(n^2-1)} \frac{|M_{\pm}|_{vc}^2}{16\pi\hbar} \left(\frac{2m_r}{\hbar^2} \right)^{\frac{3}{2}} \times \left[\sqrt{\hbar\omega - E_g^+} \frac{1}{1 + e^{\frac{\hbar\omega - E_g - \mu_F^+}{k_B T}}} - \sqrt{\hbar\omega - E_g^-} \frac{1}{1 + e^{\frac{\hbar\omega - E_g - \mu_F^-}{k_B T}}} \right]. \quad (6)$$

Equation (6) shows that, as long as such exchange-interaction-induced spin splitting is large enough to lift the quasi Fermi level (E_F^-) in the minority spin band above that (E_F^+) in the majority spin band (as depicted by the inset (a) to fig. 1), both the sign of the KR and the phase of the Larmor precession can be switched or reversed by scanning the wavelengths of the pump and probe beams simultaneously.

Figure 2 gives the KR in an extended wavelength range, which are measured at a fixed probe delay time of 100 ps under the biases of 0 V, -0.3 V, and -0.6 V by scanning the wavelength of both the pump and probe beams. After the photon energy becomes larger than the fundamental band gap (at 816.6 nm for -0.3 V, -0.6 V, and 816.7 nm for 0 V), the sign reversal of the KR from positive to negative takes place at wavelengths shorter than 816.1 nm and 815.5 nm for the biases of -0.3 V and -0.6 V, respectively. Equation (6) indicates that the sign reversal of the KR occurs when the population difference between the majority and minority spin subbands (*e.g.*, in the first subband E_1), detected by the probe photons, is inverted by scanning the photon energy $\hbar\omega$ across the quasi Fermi level E_{F1}^+ ($E_{F1}^+ = E_{g1}^+ + \mu_{F1}^+$ and $E_{F1}^- = E_{g1}^- + \mu_{F1}^-$) in the majority spin band (where spin down states reside in the present case). A similar spin splitting should also happen to the second subband E_2 as well with E_{F2}^-

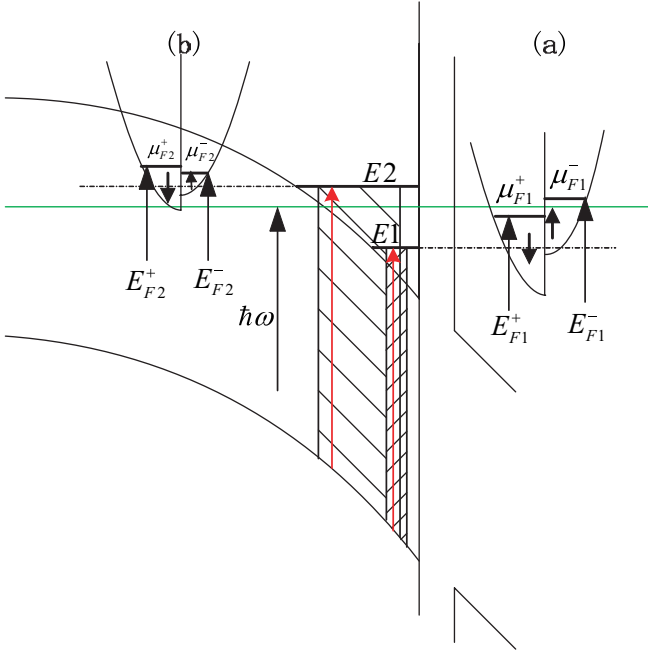


Fig. 1: (Colour on-line) energy band profile near an AlAs barrier with two subbands indicated. The hatched areas under the two subbands indicate the space where interband transitions may occur. Two arrows inside the two hatched areas represent the interband absorptions to E_2 and E_1 , excited by the same photon energy. The horizontal line, stretching to both inset (a) and (b), is the energy baseline set by photon energy. Inset (a) and (b) sketch two renormalized spin opposite bands for two subbands.

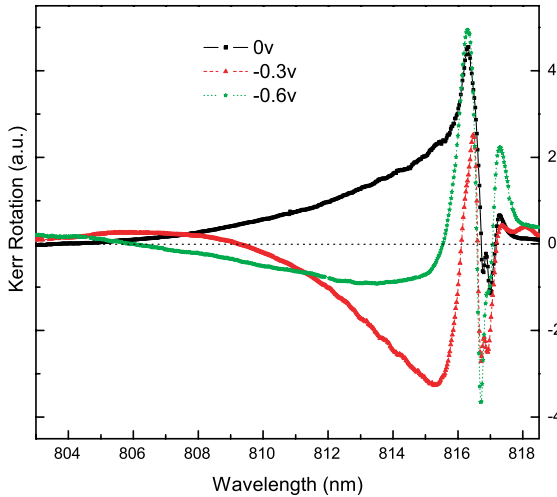


Fig. 2: (Colour on-line) KR measured by simultaneously scanning pump and probe pulses for 0 V, -0.3 V, and -0.6 V.

either below or above E_{F2}^+ , as shown by the inset (b) to fig. 1. From this physical understanding, we expect that by scanning the photon energy $\hbar\omega$ further upwards, another population inversion between the minority spin band in E_1 and the majority spin band E_2 in should occur when the probe photons break away from the first subband and begins to probe the second subband, as illustrated in fig. 1.

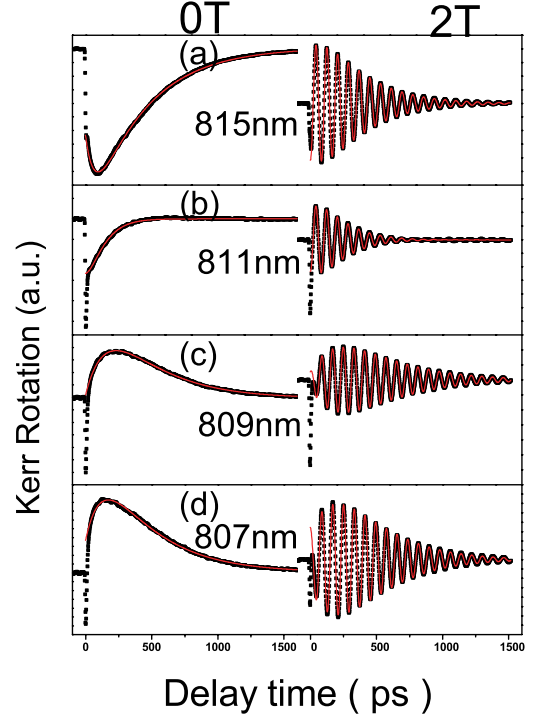


Fig. 3: (Colour on-line) KR temporal evolutions under both zero (left panel) and 2T (right panel) fields measured at wavelengths of 815 nm, 811 nm, 809 nm, and 807 nm.

Next, we use this feature to trace the appearance of the KR from the second subband. As seen from fig. 2, the KR for the biases of -0.3 V and -0.6 V switch their sign once more from negative back to positive at the wavelengths of about 810 nm and 806 nm, respectively. In fig. 3, the time evolutions of the KR are measured at wavelengths of 815 nm, 811 nm, 809 nm, and 807 nm under both a zero (the left panel) and a 2T (the right panel) field for the case of -0.3 V. When scanning the wavelength of the probe beam from 815 nm to 807 nm, a sign reversal process at the zero field (or a phase reversal process accompanied by quantum beatings at 2T) takes place around the wavelength of 810 nm. Thus, there must be two KR transient processes with the opposite signs involved in our TRKR measurements. To understand the physical origin, on one hand, the renormalized single-particle energy due to the exchange interaction is a negative correction term, and its magnitude depends on the population. Therefore, the majority and minority spin bands in both the first and second subbands descend differently. As a result, the majority spin band of E_2 may overlap with the minority spin band of E_1 in certain “resonant” energy ranges, as depicted by the horizontal line in fig. 1 (which is the energy baseline with respect to the photo-excitation). On the other hand, the effective transition regions in the space for the E_1 and E_2 subbands, as indicated by the hatched areas under E_1 and E_2 , may share the same transition energy (labeled by two arrows in fig. 1). Therefore, quantum

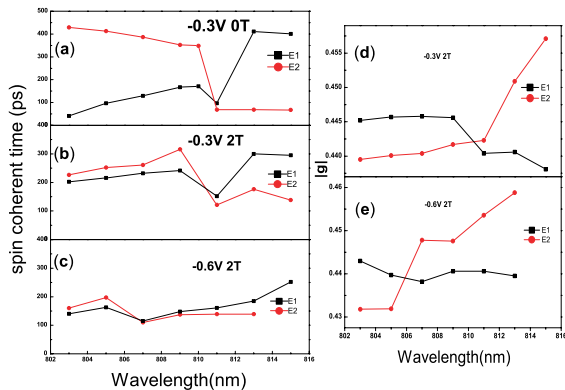


Fig. 4: (Colour on-line) (a), (b), and (c) Spin coherence times for 1st and 2nd subbands, as the wavelength varies for three different conditions: $-0.3\text{ V }0\text{ T}$, $-0.3\text{ V }2\text{ T}$, and $-0.6\text{ V }2\text{ T}$. The points are experimental results, and the lines are best fittings to the points. (d) and (e) Effective g^* factors for 1st and 2nd subbands, extracted from data in fig. 3, plotted as a function of wavelength.

beating occurs naturally between two Larmor oscillations from the first and second subbands with slightly different effective masses.

As the wavelength scans from 816 nm to 803 nm, the photon energy falls in the gap between μ_F^+ and μ_F^- in the subband. Equation (1) suggests that the KR from E_1 has a negative sign. Meanwhile, the KR from E_2 is positive and increases in magnitude when the photon energy is higher than E_{F2}^+ . Their superposition is perfectly in accordance with our observations in fig. 2 leading to a sign (or phase) reversal at about 809 nm \sim 810 nm under -0.3 V bias. Similar behaviors also appear at -0.6 V , where a sign (or a phase) reversal process at the zero field takes place around a wavelength of 806 nm. In order to properly extract two different spin coherence times and the effective g^* factors from the data, we used two different temporal exponentials for the first ($i=1$) and second ($i=2$) subbands, which are in the forms $C^i \exp[-(t-t_0)/T_2^{i*}]$ at the zero magnetic field and $C^i \exp[-(t-t_0)/T_2^{i*}] \cos[\omega_L^i(t-t_0)]$ at 2T, to fit the measured data. The fitting temporal evolutions for the zero and 2T fields are all in good agreement with the measured data and are hardly discernible from each other, as shown in fig. 3. Figure 4 gives the wavelength dependences of the spin coherent times for E_1 and E_2 under various conditions. Since the KR sign, or phase, in the wavelength range studied here is negative for the first subband and positive for the second subband, we can unambiguously distinguish the spin dynamics of E_1 band from that of E_2 band by their KR signs.

First we examine the spin coherent times T_2^{1*} for the case of the -0.3 V and zero magnetic field, as shown in fig. 4(a). By scanning the wavelength of the probe beam towards the short wavelength side, as an overall trend, the spin coherent time T_2^{1*} of E_1 decreases from 450 ps at 815 nm to 50 ps at 803 nm. However, it displays a sudden

drop at the wavelength of 811 nm. The former can be explained in the framework of the D'yakonov-Perel' (DP) decoherence mechanism [3], which increases with the wave vector in the plane, or equivalently with the photon energy in the present case. The latter discloses a new feature. At the resonant wavelength of 811 nm, the photon energy simultaneously probes the dynamics near E_{F1}^- of the spin minority band in E_1 and that close to the bottom of the spin majority band in E_2 , so the spins near the E_{F1}^- in E_1 will suffer additional exchange scattering from the spin majority band in E_2 . Such scattering is only important near the Fermi level E_{F1}^- , leading to the observed sudden drop in T_2^{1*} at 810 nm. For the spin coherence time T_2^{2*} in E_2 , it remains very low at wavelengths longer than 810 nm, and then dramatically increases afterwards. This feature is not well understood yet. As seen from fig. 1, the photons with wavelengths longer than 810 nm can only detect the spins in E_2 , which spatially dwell in the vicinity of the left boundary of Q2DES. These spins have a relatively low carrier density. We hypothesize that they may suffer exchange scattering rather effectively from the spin minority band of E_1 . When the wavelength becomes shorter than 810 nm, the spins with higher carrier density in the central part of the triangle-like quantum well make the main contribution to the KR. The inter-subband spin exchange scattering may be suppressed due to the decrease in the number of available empty final states. That, together with still small DP effect in E_2 , gives rise to a longer spin coherence time T_2^{2*} at wavelengths shorter than 810 nm.

Both T_2^{1*} and T_2^{2*} were measured under the bias of -0.3 V and the field of 2T in fig. 4(b). They show a similar variation, with sudden changes appearing at 810 nm for both T_2^{1*} and T_2^{2*} . However, because of inhomogeneous decoherence events stemming from either the fluctuation in the local effective g^* factor or the local magnetic field (*e.g.*, the Rashba and Dresselhaus fields), the differences between T_2^{1*} and T_2^{2*} are greatly suppressed, especially on the short wavelength side. The minima of T_2^{1*} and T_2^{2*} for the case of -0.6 V and 2T in fig. 4(c) both shift to 807 nm, where the phase reversal of the Larmor precessions occurs. Compared with the case of -0.3 V and 2T, the increased splitting between E_2 and E_1 by biasing seems to accelerate the intersubband scattering and tends to equalize T_2^{2*} with T_2^{1*} more efficiently.

The effective g^* factors for E_1 and E_2 are also extracted in fig. 4(d) and (e) for the biases of -0.3 V and -0.6 V , respectively. In fig. 4(d), $|g^*(E_2)|$ decreases from 0.4575 at 815 nm to 0.440 at 805 nm, while showing a step drop at about 811 nm. $|g^*(E_1)|$ remains at 0.440 when the wavelength is longer than 811 nm, then jumps to 0.445 in the range from 809 nm to 803 nm. Following $\vec{k} \cdot \vec{p}$ perturbation theory with the spin-orbit interaction included, the Landé factor near the band edge of GaAs takes the form $-0.44 + 6.3E$ for the 3D case and $-0.377 + 4.5E$ for the 2D case (where E is in the unit of eV) [7]. Thus, the Landé factor will generally show a decreasing

trend as the photon energy of the probe beam increases. The variation of $|g^*(E_2)|$ satisfies this trend. However, the steep falling of $|g^*(E_2)|$ and the sudden jumping of $|g^*(E_1)|$ from 0.440 to 0.445 are still difficult to understand. The latter may be also related to the fact that the spins detected by probe photons are spatially shifted from the left boundary to the central part of the triangle-like quantum well. It also seems that at the wavelength of about 811 nm, the resonant exchange spin coupling between the spin minority band of E_1 and the spin majority band of E_2 tends to cause band mixing to some extent, as mentioned previously. This needs to be clarified in future work.

In conclusion, by biasing a single-barrier heterostructure with a 500 nm thick GaAs layer as the absorption layer, the spin-polarized electrons, excited in the 500 nm thick GaAs layer by a circularly polarized pump pulse, drift into the vicinity of the AlAs barrier so that the second subband can be simultaneously populated to some extent with the ground subband. By simultaneously scanning the photon energy of the probe and pump beams, the sign reversal of the Kerr rotation takes place as long as the probe photons break away from the first subband and start to probe the second subband. This novel feature has been used to unambiguously distinguish and study the different spin dynamics (T_2^{1*} and T_2^{2*}) of the first and second subbands under the different conditions. In the zero magnetic field, by scanning the wavelength towards the short-wavelength side, T_2^{1*} decreases as the wave vector is gradually enlarged in accordance with the DP spin decoherence mechanism. Meanwhile, the spin coherence time T_2^{2*} in the 2nd subband E_2 remains very low at wavelengths longer than 810 nm, and then is dramatically enhanced afterwards. Eventually, T_2^{2*} probed at 803 nm becomes ten times longer than T_2^{1*} , indicating that the DP term in E_2 is much less effective than in E_1 due to the smaller wave vector there. However, the value of T_2^{2*} at 803 nm is roughly the same as the value of T_2^{1*} at 815 nm. As the inhomogeneous decoherence events (stemming from

either the fluctuation in the local effective g^* factor or the local magnetic field) set in under the magnetic field of 2T, T_2^{1*} and T_2^{2*} tend to equalize to a low value of 200 ps (150 ps) on the short wavelength side for -0.3 V (-0.6 V). A new feature has been discovered at the wavelength of 811 nm under the bias of -0.3 V (807 nm under the bias of -0.6 V) that the spin coherence times (T_2^{1*} and T_2^{2*}) and the effective factors $g^*(|g^*(E_1)|)$ and $g^*(|g^*(E_2)|)$ all display a sudden change. That is presumably attributed to the “resonant” spin exchange coupling between two spin opposite bands, occurring when the probe photons simultaneously detect the minority spin in E_1 and the majority spin in E_2 . Our result reveal new features of the spin dynamics in the second subband of Q2DES.

The authors would like to thank Z. C. NIU for the sample growth. This work was in part supported by the National Basic Research Program of China No. 2006CB932801 and No. 2007CB924904, and also by Special Research Programs of the Chinese Academy of Sciences.

REFERENCES

- [1] KIKKAWA J. M. *et al.*, *Science.*, **277** (1997) 1284; OHNO Y. *et al.*, *Phys. Rev. Lett.*, **83** (1999) 4196; GUPTA J. A. *et al.*, *Phys. Rev. B*, **59** (1999) R10421.
- [2] STICH D. *et al.*, *Phys. Rev. Lett.*, **98** (2007) 176401.
- [3] WENG M. Q. *et al.*, *Phys. Rev. B*, **70** (2004) 195318.
- [4] SAVELIEV L. G. *et al.*, *J. Phys.: Condens. Matter*, **16** (2004) 641.
- [5] ZHANG F. *et al.*, cond-mat/0711.0519 2007.
- [6] SUGANO S. *et al.*, *Magneto-Optics* (Springer-verlag, Berlin) 1999, p. 137; WALLIS R. F. *et al.*, *Many-Body Aspect of Solid State Spectroscopy* (North-Holland Physics Publishing) 1986, pp. 27–34.
- [7] YANG M. J. *et al.*, *Phys. Rev. B*, **47** (1993) 6807.